RESEARCH ARTICLE

Patterns of Vasculature in Mouse Models of Lung Cancer Are Dependent on Location

Marta Vilalta, Nicholas P Hughes, Rie Von Eyben, Amato J. Giaccia, Edward E. Graves

Department of Radiation Oncology, Molecular Imaging Program at Stanford and Bio-X Program, Stanford University, Stanford, CA, USA

Abstract

Purpose: Preclinical studies of hypoxia are generally done using ectopic xenograft tumors, which behave differently from human tumors. Our previous findings have shown that subcutaneously implanted lung tumors exhibit more hypoxia than their orthotopic implanted or spontaneous *K-ras*-induced counterparts. We hypothesize that differences in hypoxia are due to site-specific differences in vascularity and perfusion.

Procedures: To compare the presence and functionality of vessels in these tumor models, we studied vascular perfusion in vivo in real time.

Results: Orthotopically implanted and spontaneous *K-ras*-induced lung tumors showed elevated perfusion, demonstrating vasculature functionality. Little contrast agent uptake was observed within the subcutaneously implanted tumors, indicating vascular dysfunction. These findings were corroborated at the microscopic level with Hoechst 33342 and Meca-32 staining.

Conclusions: From these observations, we concluded that differences in hypoxia in experimental models is related to vessel perfusion. Thus, appropriate selection of preclinical lung tumor models is essential for the study of hypoxia, angiogenesis and therapies targeting these phenomena.

Key words: Preclinical models of cancer, Xenograft models, Non-invasive imaging in animal models, Tumor microenvironment, Vasculature

Introduction

Blood vessels play a fundamental role in cancer progression, as they are necessary for the growth and spread of the cancer cells in the tumors. It has been shown that the development of new blood vessels in solid tumors, either by local sprouting of existing blood vessels (angiogenesis) or by recruitment of vascular progenitor cells (postnatal vasculogenesis), results in neovasculature that is both structurally and functionally abnormal [1]. The endothelial cells surrounding these vessels have a divergent morphology [2–4]. This dysfunctional vasculature leads to chaotic blood flow that in turn creates a hypoxic and acidic tumor microenvironment with elevated interstitial fluid pressure (IFP) [5]. This increased IFP in solid tumors acts as a barrier to drug delivery [6]. All of these characteristics contribute to the leakiness of tumor vessels, which are an order of magnitude more permeable than normal vessels [5]. These unique properties of angiogenic tumor vasculature have encouraged the development of therapeutic strategies targeting them, including vascular disrupting agents and anti-angiogenic therapies. Some of these treatments have been observed to transiently improve tumor blood flow. This vascular normalization was postulated almost 10 years ago [1] and has been exploited to enhance the action of concurrent treatments including radiotherapy and chemotherapy [7, 8].

Angiogenesis is stimulated by hypoxia [7, 9–11], which reduces the efficacy of radiotherapy. In addition, studies have shown that hypoxia also accentuates tumor aggressiveness and metastasis [12, 13]. However, much of our knowledge of the effects of hypoxia is based on preclinical

Correspondence to: Edward Graves; *e-mail:* egraves@stanford.edu

studies using xenografted human tumors implanted ectopically in the subcutis of mice. It is known that these models exhibit important differences in behavior from human tumors [14]. Differences in vascular transport have been observed when comparing different tumor models, grown either orthotopically or ectopically. However, there remains significant controversy on this topic. Some studies have observed reduced transvascular transport of large macromolecules when tumors are grown orthotopically in the cranial microenvironment compared to their ectopic subcutis-implanted counterparts [15]. However, higher vascular permeability and higher accumulation of nanocarriers has been observed when tumors were grown orthotopically in the liver and breast compared to their ectopic subcutaneous counterparts [16, 17]. Other discrepancies, such as growth rate, metastatic potential, and efficacy of treatment, have also been demonstrated across different tumor models. For example, orthotopic implantation of PC-3 cells resulted in significantly more lymph node metastases compared to subcutaneous implantation [18]. Also, a number of tumor types have been shown to metastasize in nude mice only if they are orthotopically implanted [19].

We have reported previously that subcutaneously implanted lung tumors in mice exhibit significant hypoxia while both orthotopic and spontaneous tumors are better oxygenated. Furthermore, when these tumor models were treated with the hypoxic cytotoxin PR-104, only subcutaneously implanted tumors exhibited DNA damage [20]. These observations raise the question of how these differences in hypoxia across models of genetically similar or identical tumors occur. One hypothesis that could explain these differences in hypoxia is due to differences in vascularity and perfusion between these tumor systems [21]. The aim of the present study was to compare vessel presence and functionality in these preclinical models of lung cancer. In order to accomplish this, we used models of lung cancer generated spontaneously or from tumor cells implanted orthotopically or ectopically and analyzed them with dynamic contrast-enhanced magnetic resonance (DCE-MRI), a technique that enables non-invasive interrogation of the tissue vascular environment and can assess vascular permeability in tumors [22, 23].

Materials and Methods

Animal Models

All animal experiments were done according to a protocol approved by the Institutional Animal Care and Use Committee. Expression of the K-ras oncogene in the lung cells from mice bearing a Lox-Stop-Lox-K-ras gene was induced using a nasally delivered adeno-Cre construct as described previously [24], resulting in focal K-ras-positive lung lesions within 12–15 weeks of infection. Tumors generated in a subset of K-ras-induced mice were harvested and used to produce cell lines in vitro, which were grown and then injected to mice of the same background as the Lox-stop-Lox-K-ras

transgenic mice in order to produce subcutaneous ectopic models (10^6 tumor cells in 50 µl of matrigel) and orthotopic lung tumors as previously described (10^6 tumor cells) [25].

Micro-X-Ray Computed Tomography Imaging

Tumor formation and precise location in the lungs were monitored by Micro-X-ray computed tomography (microCT) scans using an eXplore Locus RS120 microCT scanner (GE Health Care, Milwaukee, WI) prior to MRI imaging. The acquisition included 360 views spaced over 360°, resulting in a spatial resolution of 8 µm. The scan time was 8 min. Data were analyzed with the GEHC MicroView software.

Dynamic Contrast-Enhanced Magnetic Resonance Imaging

Mice were anesthetized with 2 % isoflurane and a catheter (Vevo® MicroMarker™ TVA, VisualSonics, Toronto, Canada), attached to 5 ft of tubing (0.018″ ID × 0.036″ OD) (BPE-T25, Salomon Scientific, San Antonio, TX), and loaded with 150 µl of heparin +250 µl of PBS 1×, that was implanted in the tail vein. The mice were then placed on an MRI-compatible bed for scanning. Mice were imaged using a 7.0 T MRI scanner (MR901, Agilent Technologies, Santa Clara, CA). For the T2-weighted scan, we imaged the thoracic area, acquiring 10 slices with a thickness of 0.75 mm. For the dynamic contrast enhanced scan, 100 µl of gadolinium-based contrast agent (MAGNEVIST®) at a dose of 0.1 mmol/kg body weight was injected slowly through the catheter over a period of 30 s beginning after four time points (26 s) of the DCE scan. We used a temporal resolution of 6.5 s, with a total of 51 time points, resulting in a total scan time of 5.5 min (TR/TE = 5/0.9 ms)."

Calculations

RT_Image [26] was used to define regions of interest (ROI) from the T2 images, which were aligned with the DCE images. Contrast agent concentration curves were calculated from both the DCE images and the inversion recovery images, and the initial area under the gadolinium-time curve at 60 s ($IAUGC_{60}$) was determined from these curves [27].

Immunohistochemistry

After DCE-MRI imaging, Hoechst 33342 (Sigma-Aldrich, St. Louis, MO) was injected intravenously to the mice to a dose of 15 mg/kg body weight. One minute after injection, animals were euthanized by CO_2 inhalation and the lungs and subcutaneous tumors (if any) were excised. The lungs were inflated and fixed using a 10 % neutral buffer formalin solution (Thermo Fisher Scientific, Waltham, MA), while subcutaneous tumors were rinsed in PBS and fixed with a 10 % neutral buffer formalin solution for 24 h. Both the lungs and the tumors were then embedded in paraffin and cut into 4-µm sections. The sections were directly imaged for Hoechst 33342 and stained for Meca-32 (BD Pharmingen, San Jose, CA) and carbonic anhydrase IX (CAIX)
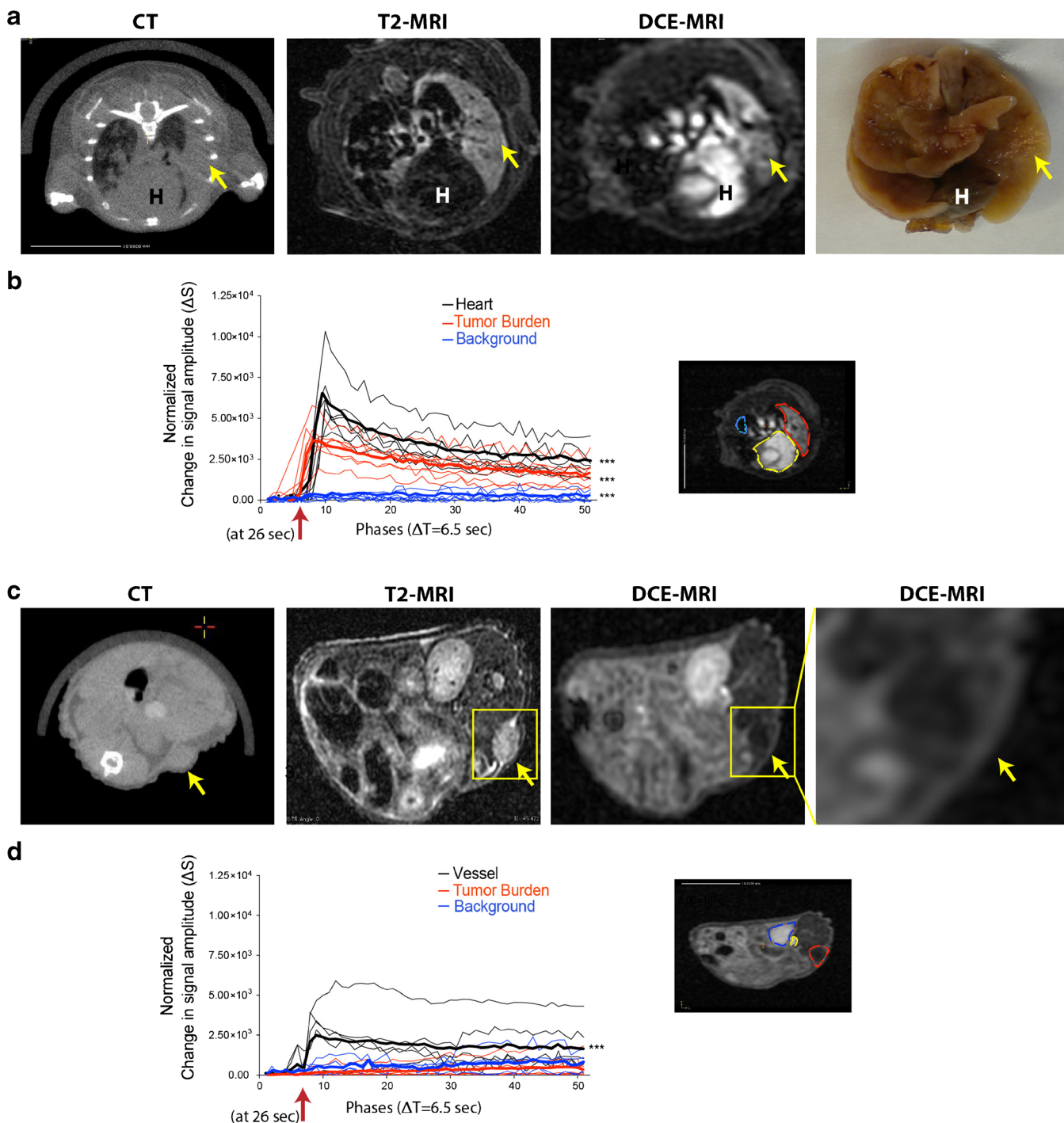
Fig. 1 Spontaneous *K-ras*-induced lung tumors showed greater contrast agent uptake compared to the subcutaneously injected counterparts. **a** Spontaneous *K-ras*-induced lung tumors were monitored with X-ray CT (*left panel*). T2-MRI (*left middle panel*) was performed before contrast agent injection (Gadolinium-DTPA) followed by DCE-MRI (*right middle panel*) (*N* = 7). *Yellow arrows* indicate the location of the tumor, and the heart is indicated as *H*. **b** Contrast agent uptake quantification (presented as normalized change in signal amplitude, ΔS) for specific regions of interest (ROI) including background (*blue*), tumor burden (*red*), and heart (*black*). *Bold lines* represent the mean of all regions (N = 7 for each organ). The *red arrow* indicates the time of contrast agent injection. The image on the *right* shows the exact ROI used to quantify the contrast agent uptake from the tumor (*red*), background (*blue*) and heart (*yellow*). **c** Ectopic subcutaneous implanted tumors were monitored with CT (*left panel*). T2-MRI (*left middle panel*) was performed before contrast agent injection followed by DCE-MRI (*right middle panel*) (*N* = 5). *Yellow arrows* indicate the location of the tumor, and the *yellow box* denotes the magnified area. **d** Contrast agent uptake quantification (presented as change in signal amplitude, ΔS) for a specific ROI including background (*blue*), tumor (*red*), and vessel (*black*). *Bold lines* represent the mean of all regions (*N* = 5 for each group). The *red arrow* indicates the time of contrast agent injection. The image on the *right* shows the ROI position used to quantify the contrast agent uptake from the tumor (*red*), background (*blue*), and vessel (*yellow*) (***P < 0.0001) (color figure online).
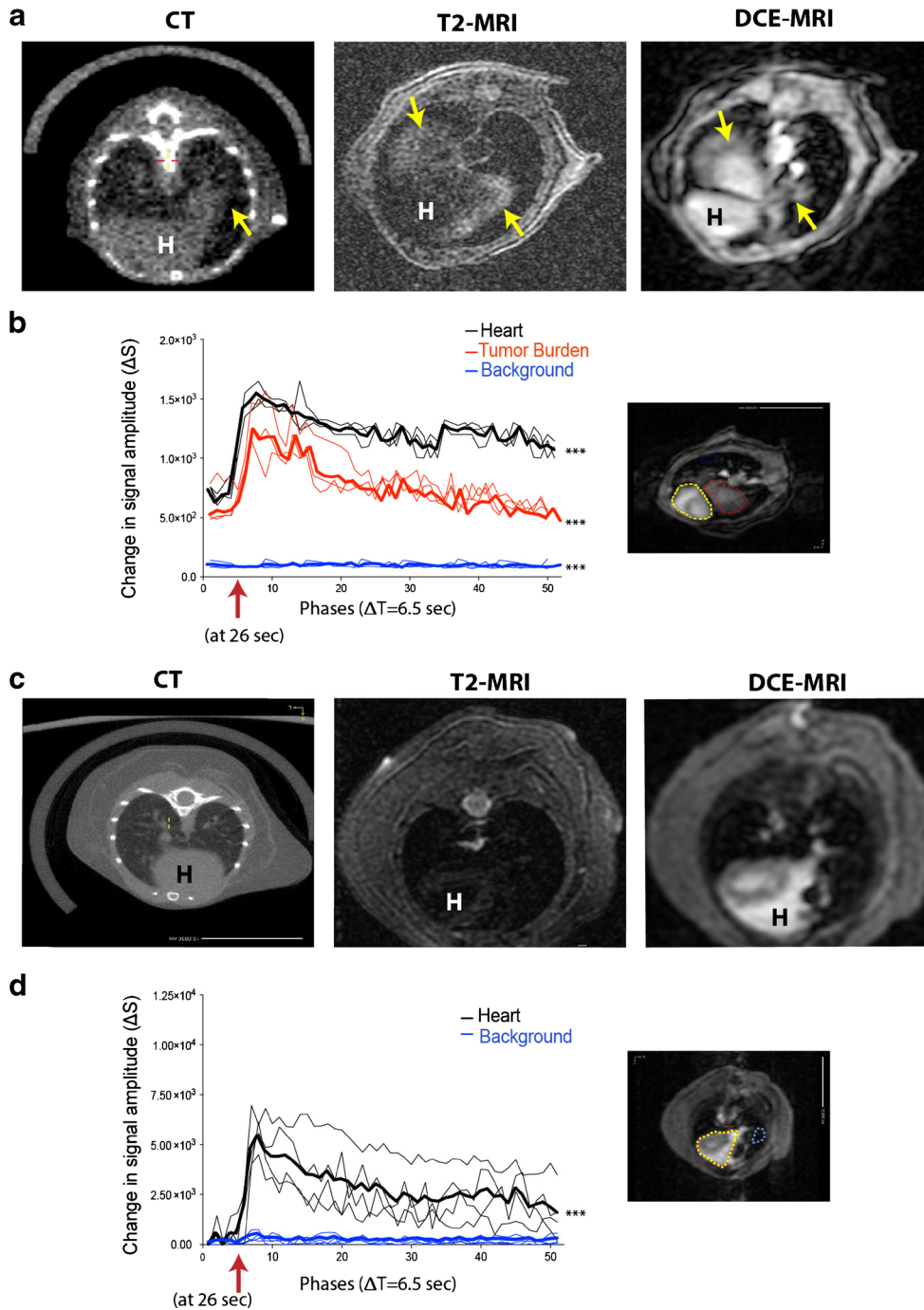
Fig. 2 Orthotopic implanted lung tumors showed similar uptake compared to spontaneous *K-ras*-induced lung tumors, while regular lung tissue showed no contrast agent uptake. **a** Orthotopically implanted lung tumors were monitored with X-ray CT (*left panel*). T2-MRI (*middle panel*) was performed before contrast agent injection (Gadolinium-DTPA) followed by DCE-MRI (*right panel*) (*N* = 3). *Yellow arrows* indicate the location of the tumor, and the heart is indicated as *H*. **b** Contrast agent uptake quantification (presented as normalized change in signal amplitude, ΔS) for specific regions of interest (ROI) including background (*blue*), tumor burden (*red*), and heart (*black*). *Bold lines* represent the mean of all regions (*N* = 3 for each organ). The *red arrow* indicates the time of contrast agent injection. The image on the *right* shows the exact ROI used to quantify the contrast agent uptake from the tumor (*red*), background (*blue*), and heart (*yellow*). **c** Control mice were monitored with CT (*left panel*) to image the pulmonary area. T2-MRI (*middle panel*) was performed before contrast agent injection followed by DCE-MRI (*right panel*) (*N* = 4). The heart position is indicated as *H*. **d** Contrast agent uptake quantification for specific regions of interest including background (*blue*) and heart (*black*). *Bold lines* represent the mean of all regions (*N* = 4 for each organ). The red *arrow* indicates the time of the contrast agent injection. The image on the *right* shows the exact ROI position used to quantify the contrast agent uptake from the background (*blue*) and heart (*yellow*) (***$P < 0.0001$) (color figure online).

a

b

c

d
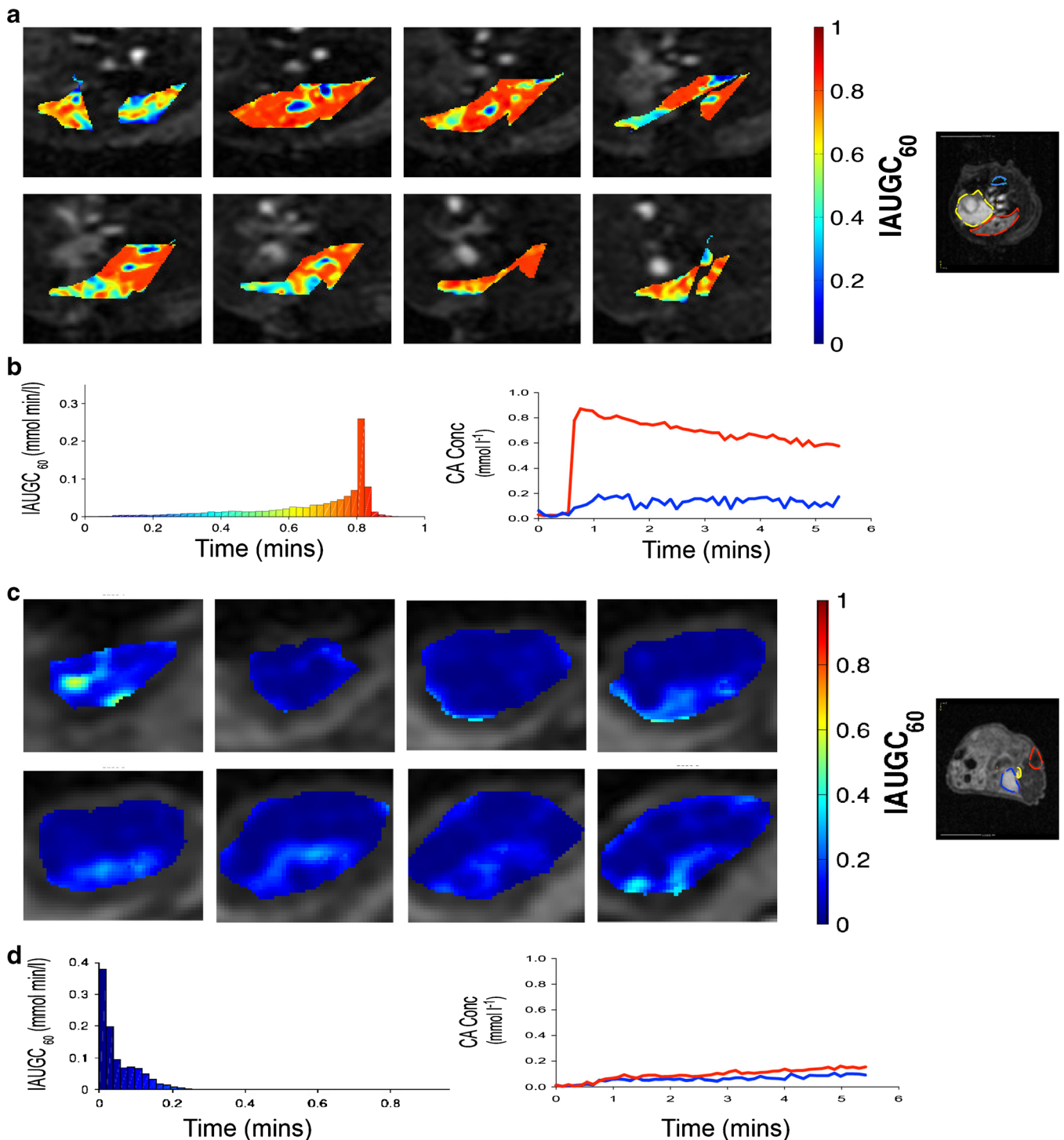
Fig. 3 Parametric maps show that spontaneous K-ras-induced lung tumor models accumulate higher concentrations of contrast agent than their subcutaneously implanted counterparts. **a** Initial area under the gadolinium-time curve at 60 s ($IAUGC_{60}$) parametric maps for a representative mouse bearing a spontaneous K-ras-induced lung tumor. **b** Histogram showing the $IAUGC_{60}$ from the parametric maps. On the *right*, the contrast agent (CA) concentration curve from the DCE-MRI data over the entire tumor region is shown. **c** $IAUGC_{60}$ parametric maps for a representative mouse bearing a subcutaneously implanted ectopic lung tumor. **d** Histogram showing the $IAUGC_{60}$ from the parametric maps. On the *right*, the CA concentration curve from the DCE-MRI data over the entire tumor region is shown.
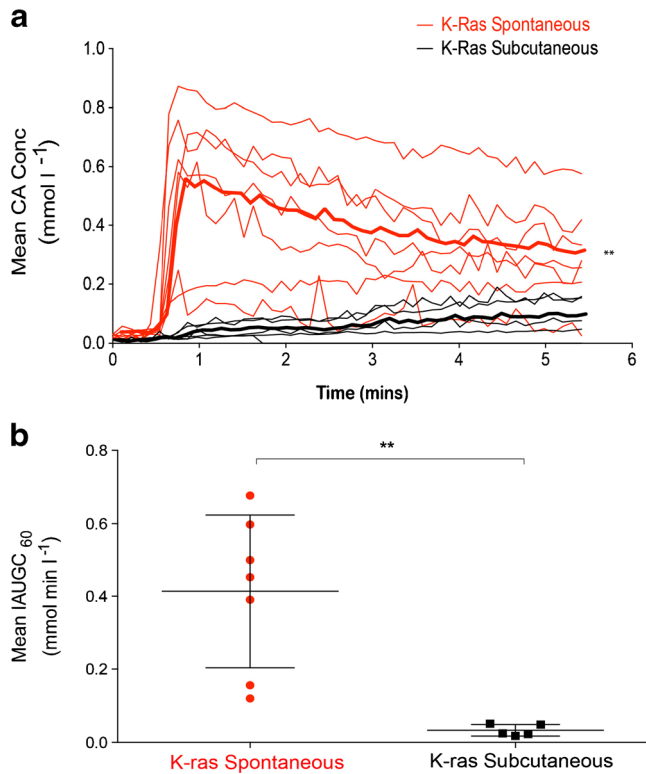
Fig. 4 Spontaneous lung tumor models show a higher contrast agent extravasation than their subcutaneously implanted counterparts. **a** Contrast agent concentration curves for both spontaneous lung tumors (*red*) and subcutaneously injected tumors (*black*). *Bold lines* indicate the mean for each tumor type. **b** $IAUGC_{60}$ mean comparison for the spontaneous lung tumors (*red*) and the subcutaneous (*black*) (**P < 0.01) (color figure online).

Statistical Analysis

In order to compare the differences in contrast agent uptake for the different tumors models, data were analyzed using a mixed effects model with repeated measures over time within each mouse. Organ was included as a fixed effect, and the contrast agent level in each organ (tumor, background, and vessel or heart) was compared in an ad hoc analysis with a Tukey adjustment for multiple comparisons.

A multivariate ANOVA was used to compare the different immunohistochemistry (IHC) postmortem staining, Hoechst 33342 and Meca-32, and DCE responses for spontaneous and subcutaneous groups. Finally, a two-sided *t* test was used to compare Hoechst 33342 and Meca-32 staining of the edge versus the middle of the tumors.

Results

Spontaneous Lung K-ras-Induced Tumors Show Increased Perfusion Relative to Subcutaneously Implanted Lung Tumors

To investigate whether the vasculature formed in different mouse models of lung cancer possessed unique functionality, we

performed DCE-MRI in both spontaneous *K-ras*-induced lung tumors and subcutaneously implanted ectopic tumors. Prior to DCE-MRI imaging, we also performed T2-weighted MRI (T2-MRI), as well as X-ray computed tomography (CT), in order to validate both the presence, location, and size of the tumors. From the DCE-MRI images and corresponding quantification of contrast agent uptake over time, we observed a large increase in gadolinium uptake in lung tumors after contrast injection, whereas little signal increase was detected in the subcutaneous tumors (Fig. 1a–d). This difference in contrast agent uptake suggested that vasculature in the subcutaneous tumors was either dysfunctional or insufficient relative to the spontaneous lung tumors. When the DCE-MRI subcutaneous tumor image was magnified, a small area at the rim of the tumor showed some gadolinium uptake, suggesting that some functional vasculature may be located in that area, supporting both the blood supply and the growth of the tumor (Fig. 1c, right panel).

In order to verify the success of contrast agent injection, we also quantified the change in signal amplitude from the heart for the spontaneously *K-ras*-induced tumors or from a large vessel or perfused organ for the subcutaneous tumors. These reference organs were chosen based on their location within the imaging field of view. Significant increases in imaging signal were observed in each animal studied regardless of tumor type, demonstrating that the contrast injections were each performed successfully.

As an additional control, we imaged transgenic animals of the same strain as the spontaneous tumor-bearing mice, but which were not administered adenovirus containing the Cre recombinase, in order to stimulate tumor formation. The thorax of these non-tumor bearing mice was scanned as before. From the images and quantification, we observed no increase in signal after contrast injection in the lungs. Only the heart exhibited gadolinium uptake, demonstrating that the changes in signal amplitude shown in Fig. 1a–c were specific to the tumors growing in these mice (Fig. 2c, d).

In order to determine if the difference in contrast agent uptake was due to the different site of growth or because of the inoculation procedure itself, we injected cells orthotopically in the lungs and followed the same imaging protocol. We observed a contrast agent uptake pattern similar to that of the spontaneous *K-ras*-induced lung tumors, suggesting that the location and not the implantation procedure drives vascular functionality in these tumors (Fig. 2a, b).

In Vivo Contrast Agent Uptake Differences Between Different Tumor Models of Lung Cancer Correlate with the Degree of Signal Accumulation

Parametric maps were created from the DCE-MRI data showing the $IAUGC_{60}$. This composite measure of vascular permeability and tumor blood flow was generated for both tumor models. The intensity of the parametric maps was significantly increased in the spontaneous lung tumors as compared to the subcutaneous tumors (Fig. 3a, c). While the mean contrast agent concentration uptake
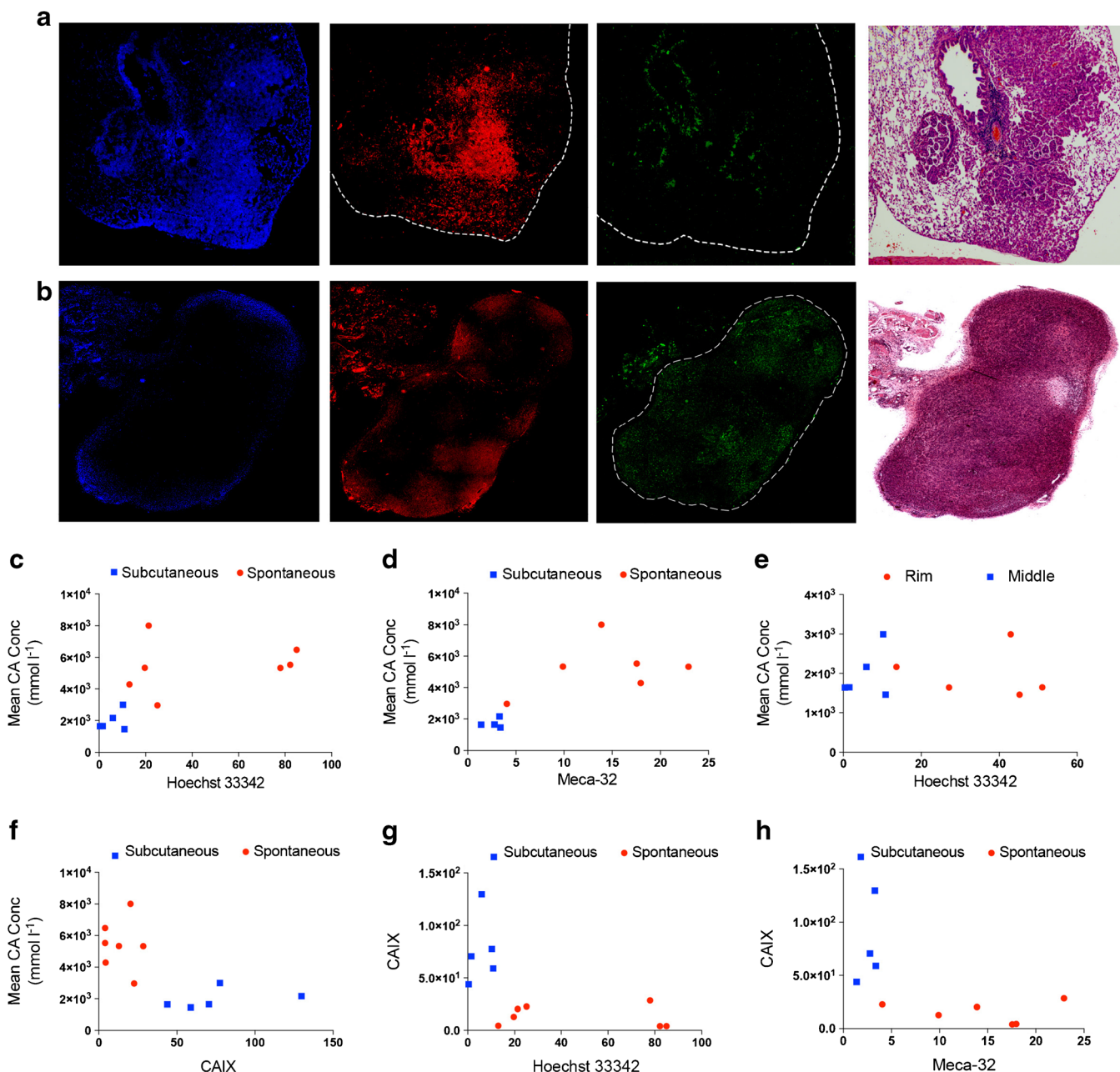
Fig. 5 Histologic analysis demonstrates that spontaneous lung tumors have more functional vasculature. **a** Hoechst 33342 (*blue*), Meca-32 (*red*), CAIX (*green*), and H&E staining of a representative mouse bearing a spontaneous lung tumor. **b** Hoechst 33342 (*blue*), Meca-32 (*red*), CAIX (*green*), and H&E staining of a representative mouse bearing a subcutaneously implanted tumor. **c** Correlation between Hoechst 33342 intensity and contrast agent concentration for both spontaneous and subcutaneous lung tumors ($P < 0.005$). **d** Correlation between Meca-32 intensity and contrast agent concentration for both spontaneous and subcutaneous lung tumors ($P < 0.05$). **e** Correlation between Hoechst 33342 intensity comparing the rim and the center of the subcutaneous implanted tumors ($P < 0.05$)." **f** Correlation between CAIX intensity and contrast agent concentration for both spontaneous and subcutaneous lung tumors ($P < 0.005$). **g** Correlation between Hoechst 33342 intensity and CAIX intensity for both spontaneous and subcutaneous lung tumors ($P < 0.005$). **h** Correlation between Meca-32 intensity and CAIX intensity for both spontaneous and subcutaneous lung tumors ($P < 0.005$) (color figure online).

over the first 60 s after injection reached 0.7 mmol/l for the spontaneous *K-ras*-induced tumors ($N = 7$), only 0.03 mmol/l was measured for the subcutaneous tumors ($N = 5$) (Fig. 3b, d). Contrast agent-concentration curves as a function of time for every tumor voxel over the measurement period of 5.5 min

showed a large degree of variation, even within a single tumor type (Fig. 4a); however, the increased uptake in the spontaneous lung tumor models was apparent and statistically significant.

When comparing IAUGC$_{60}$ mean values for both tumor models, we observed a significant difference between the

measurements. This suggests that the vasculature in the spontaneous lung tumor models allowed more signal accumulation, thus more contrast agent extravasation than their subcutaneous counterparts (Fig. 4b).

Histologic Analysis Demonstrates Increased Vascularization and Perfusion in Spontaneous K-ras-Induced Lung Tumors Relative to Subcutaneous Ectopic Tumors

In order to assess the functionality of vasculature across the different tumor types, we administered Hoechst 33342 intravenously to tumor-bearing mice prior to sacrifice. In the subcutaneously injected group of tumors, Hoechst 33342 staining was observed only at the rim of the tumors, while positive staining was detected throughout tumors growing in the lungs (Fig. 5a, b). These findings agree with the DCE-MRI results and demonstrate that blood vessels were more functional at the time of the dye perfusion in the spontaneous K-ras-induced lung tumor models relative to the subcutaneously injected group (Fig. 5c).

We also performed MECA-32 staining, which exclusively stains for the endothelial cells but not for the surrounding pericytes [28], to characterize the presence of the blood vessels within the tumor masses (Fig. 5a, b). We found positive MECA-32 staining only at the rim of the subcutaneous tumors while it was present throughout the lung tumors. This pattern correlated with the Hoechst 33,342 staining pattern, further corroborating that the difference in contrast agent uptake is due to differences in both blood vessel presence as well as functionality (Fig. 5c–e). Furthermore, CAIX staining showed a significant difference in the hypoxia pattern between these models, which contrasted perfectly with MECA-32 and Hoechst 33342 staining patterns (Fig. 5g, h).

Discussion

As we have shown previously, investigations of tumor hypoxia, and specifically the performance of hypoxia-targeted therapies and their translational potential, are inextricably tied to the models in which these investigations are conducted. In particular, lung cancer tumor models implanted either orthotopically in the lung or ectopically in the subcutis showed differences in hypoxia that affected the therapeutic efficacy of chemotherapy drugs targeting hypoxic cells [20]. Thus, such therapies will be preferentially effective in subcutaneous tumor models that have poor oxygenation and less effective in orthotopic and spontaneous disease models that may be more physiologically relevant to human disease. In the current study, we found that lung tumors growing in their native environment formed vessels that were more functional than those formed by the same tumor cells growing subcutaneously in a foreign environment. Using DCE-MRI, we monitored vascular permeability

in order to quantify the perfusion and extravasation of a small molecule gadolinium contrast agent non-invasively. This modality has been used previously to grade the aggressiveness of the tumors and to quantitatively interrogate their vascularity [22]. Our DCE-MRI findings agreed with ex vivo histologic studies, where we stained for Meca-32 and Hoechst 33342 in order to visualize the presence and the functionality of the vasculature, respectively. The results of the present study suggest that the discrepancy in the hypoxia level, measured by CAIX expression, in these different tumor models is a consequence of the differences in vessel formation and functionality. Overall, our results demonstrate the influence that a specific preclinical tumor system can play in the physiologic behavior of the model as a whole, which may be of great importance in the evaluation of the efficacy of therapies studied using these tumor models.

To date, no preclinical tumor model perfectly recapitulates human disease because of differences across species, tumor environment, and immune response [29]. Furthermore, it has been shown that the site of the tumor implantation can be critical, since tumor-host interactions and tumor microenvironment can modulate tumor development, disease progression, and response to therapy [30, 31]. Some of these issues can be overcome by using genetically engineered mouse models (GEMMs), which mimic the process of carcinogenesis and therefore can yield animal tumors that more accurately reflect the behavior of human tumors observed in clinical trials [32, 33]. GEMM models are slow growing and costly; therefore, ectopically implanted xenograft tumors remain widespread in their use and can provide useful data on basic and translational biology, such as to study patient derived biopsies, provided their limitations are properly considered. However, the pervasive use of ectopic subcutaneous xenograft tumors over the years as a preclinical model has resulted in a discordance between preclinical research and clinical trials, especially in the case of targeted therapeutics [34–37], thus, these models should be further investigated before being broadly used as informative tool for the efficacy and toxicity of certain compounds. Ideally, a range of preclinical models should be used to validate the efficacy of certain drugs before moving forward to human use [38].

It is well known that the content of newly formed immature vessels, which are poorly differentiated and have a leaky endothelium, is extremely high in rapidly growing preclinical tumor models compared to the spontaneous, more slowly growing tumors in humans [22, 39]. Tumor vascular permeability as well as the lack of functional lymphatic vessels influences angiogenesis, tumor growth and metastasis, and drug delivery [40–42]. Studies from Ho et al. demonstrated that tumors grown orthotopically in the mammary fad pad exhibit a higher vascular size and density and thinner basement membranes compared to subcutaneously injected ones [17]. Similarly, prostate tumors have increased vascular density, vessel permeability, oxygenation,

and VEGF expression when grown orthotopically as compared to in the subcutis [43]. Other studies have observed that the interstitial fluid pressure of intramuscularly implanted tumors is significantly higher compared to orthotopically implanted tumors [6]. In a similar way, a difference in the vascular network has been shown in models of lung cancer. Downey et al. [37] demonstrated the preferential sensitivity of subcutaneous tumor models to a vascular disrupting agent relative to primary spontaneous tumors and metastatic lesions. Ex vivo 3D microCT images showed large differences in the vascular structure and thickness as well as internal avascular areas, demonstrating again differences in the structure of the tumor vascular network across different tumor sites.

The data presented here not only provide a valid explanation for the failure of some studies based on ectopic subcutaneous models but also give essential information on the structure and functionality of the vasculature in different tumor models of lung cancer. As far as we know, this is the first study to demonstrate the difference in vasculature functionality in different lung tumor models in vivo and in real time.

In conclusion, the use of preclinical models of human malignancies that reflect the disease more closely, such as orthotopic implantation or spontaneous *K-ras*-induced tumors, should be emphasized in certain studies. Particularly, with preclinical models of lung cancer, we demonstrated that ectopically implanted tumors are not appropriate models for investigations that target either hypoxia or angiogenesis and for treatments that need functional vasculature in order to be delivered, as vasculature differences between models may affect the results of therapeutic trials. Based on the observations mentioned above, judicious selection of preclinical models is essential in order to maximize the translational relevance of these investigations.

Compliance with Ethical Standards. All animal experiments were done according to a protocol approved by the Institutional Animal Care and Use Committee.

Conflict of Interest

The authors declare that they have no conflict of interest.

References

1. Jain RK (2005) Normalization of tumor vasculature: an emerging concept in antiangiogenic therapy. Science 307:58–62
2. McDonald DM, Foss AJ (2000) Endothelial cells of tumor vessels: abnormal but not absent. Cancer Metastasis Rev 19:109–120
3. Morikawa S, Baluk P, Kaidoh T et al (2002) Abnormalities in pericytes on blood vessels and endothelial sprouts in tumors. Am J Pathol 160:985–1000
4. Hashizume H, Baluk P, Morikawa S et al (2000) Openings between defective endothelial cells explain tumor vessel leakiness. Am J Pathol 156:1363–1380
5. Carmeliet P, Jain RK (2000) Angiogenesis in cancer and other diseases. Nature 407:249–257
6. Lunt SJ, Kalliomaki TM, Brown A et al (2008) Interstitial fluid pressure, vascularity and metastasis in ectopic, orthotopic and spontaneous tumours. BMC Cancer 8:2
7. Moeller BJ, Richardson RA, Dewhirst MW (2007) Hypoxia and radiotherapy: opportunities for improved outcomes in cancer treatment. Cancer Metastasis Rev 26:241–248
8. Moding EJ, Kastan MB, Kirsch DG (2013) Strategies for optimizing the response of cancer and normal tissues to radiation. Nat Rev Drug Discov 12:526–542
9. Shweiki D, Itin A, Soffer D, Keshet E (1992) Vascular endothelial growth factor induced by hypoxia may mediate hypoxia-initiated angiogenesis. Nature 359:843–845
10. Marti HJ, Bernaudin M, Bellail A et al (2000) Hypoxia-induced vascular endothelial growth factor expression precedes neovascularization after cerebral ischemia. Am J Pathol 156:965–976
11. Moeller BJ, Cao Y, Vujaskovic Z et al (2004) The relationship between hypoxia and angiogenesis. Semin Radiat Oncol 14:215–221
12. Young SD, Marshall RS, Hill RP (1988) Hypoxia induces DNA overreplication and enhances metastatic potential of murine tumor cells. Proc Natl Acad Sci U S A 85:9533–9537
13. Brown JM (1999) The hypoxic cell: a target for selective cancer therapy–eighteenth Bruce F. Cain Memorial Award lecture. Cancer Res 59:5863–5870
14. Killion JJ, Radinsky R, Fidler IJ (1998) Orthotopic models are necessary to predict therapy of transplantable tumors in mice. Cancer Metastasis Rev 17:279–284
15. Hobbs SK, Monsky WL, Yuan F et al (1998) Regulation of transport pathways in tumor vessels: role of tumor type and microenvironment. Proc Natl Acad Sci U S A 95:4607–4612
16. Fukumura D, Yuan F, Monsky WL et al (1997) Effect of host microenvironment on the microcirculation of human colon adenocarcinoma. Am J Pathol 151:679–688
17. Ho KS, Poon PC, Owen SC, Shoichet MS (2012) Blood vessel hyperpermeability and pathophysiology in human tumour xenograft models of breast cancer: a comparison of ectopic and orthotopic tumours. BMC Cancer 12:579
18. Waters DJ, Janovitz EB, Chan TC (1995) Spontaneous metastasis of PC-3 cells in athymic mice after implantation in orthotopic or ectopic microenvironments. Prostate 26:227–234
19. Glinskii AB, Smith BA, Jiang P et al (2003) Viable circulating metastatic cells produced in orthotopic but not ectopic prostate cancer models. Cancer Res 63:4239–4243
20. Graves EE, Vilalta M, Cecic IK et al (2010) Hypoxia in models of lung cancer: implications for targeted therapeutics. Clin Cancer Res 16:4843–4852
21. Maity A, Koumenis C (2010) Location, location, location-makes all the difference for hypoxia in lung tumors. Clin Cancer Res 16:4685–4687
22. McDonald DM, Baluk P (2002) Significance of blood vessel leakiness in cancer. Cancer Res 62:5381–5385
23. Jackson A, O'Connor JP, Parker GJ, Jayson GC (2007) Imaging tumor vascular heterogeneity and angiogenesis using dynamic contrast-enhanced magnetic resonance imaging. Clin Cancer Res 13:3449–3459
24. Jackson EL, Willis N, Mercer K et al (2001) Analysis of lung tumor initiation and progression using conditional expression of oncogenic K-ras. Genes Dev 15:3243–3248
25. Maatta AM, Makinen K, Ketola A et al (2008) Replication competent Semliki Forest virus prolongs survival in experimental lung cancer. Int J Cancer 123:1704–1711
26. Graves EE, Quon A, Loo BW Jr (2007) RT_Image: an open-source tool for investigating PET in radiation oncology. Technol Cancer Res Treat 6:111–121
27. Tofts PS, Brix G, Buckley DL et al (1999) Estimating kinetic parameters from dynamic contrast-enhanced T(1)-weighted MRI of a diffusable tracer: standardized quantities and symbols. J Magn Reson Imaging 10:223–232
28. Nolan-Stevaux O, Truitt MC, Pahler JC et al (2010) Differential contribution to neuroendocrine tumorigenesis of parallel egfr signaling in cancer cells and pericytes. Genes Cancer 1:125–141
29. Jung J (2014) Human tumor xenograft models for preclinical assessment of anticancer drug development. Toxicol Res 30:1–5
30. Field SB, Needham S, Burney IA et al (1991) Differences in vascular response between primary and transplanted tumours. Br J Cancer 63:723–726
31. Kerbel RS (2000) Tumor angiogenesis: past, present and the near future. Carcinogenesis 21:505–515

32. Frese KK, Tuveson DA (2007) Maximizing mouse cancer models. Nat Rev Cancer 7:645–658

33. Singh M, Murriel CL, Johnson L (2012) Genetically engineered mouse models: closing the gap between preclinical data and trial outcomes. Cancer Res 72:2695–2700

34. Kerbel RS (2003) Human tumor xenografts as predictive preclinical models for anticancer drug activity in humans: better than commonly perceived-but they can be improved. Cancer Biol Ther 2:S134–S139

35. Dutt A, Wong KK (2006) Mouse models of lung cancer. Clin Cancer Res 12:4396s–4402s

36. Olive KP, Jacobetz MA, Davidson CJ et al (2009) Inhibition of hedgehog signaling enhances delivery of chemotherapy in a mouse model of pancreatic cancer. Science 324:1457–1461

37. Downey CM, Aghaei M, Schwendener RA, Jirik FR (2014) DMXAA causes tumor site-specific vascular disruption in murine non-small cell lung cancer, and like the endogenous non-canonical cyclic dinucleotide STING agonist, 2′3′-cGAMP, induces M2 macrophage repolarization. PLoS One 9:e99988

38. Cai KX, Tse LY, Leung C et al (2008) Suppression of lung tumor growth and metastasis in mice by adeno-associated virus-mediated expression of vasostatin. Clin Cancer Res 14:939–949

39. Benjamin LE, Golijanin D, Itin A et al (1999) Selective ablation of immature blood vessels in established human tumors follows vascular endothelial growth factor withdrawal. J Clin Invest 103:159–165

40. Dvorak HF, Nagy JA, Dvorak JT, Dvorak AM (1988) Identification and characterization of the blood vessels of solid tumors that are leaky to circulating macromolecules. Am J Pathol 133:95–109

41. Dreher MR, Liu W, Michelich CR et al (2006) Tumor vascular permeability, accumulation, and penetration of macromolecular drug carriers. J Natl Cancer Inst 98:335–344

42. Shuhendler AJ, Prasad P, Cai P et al (2013) Matrigel alters the pathophysiology of orthotopic human breast adenocarcinoma xenografts with implications for nanomedicine evaluation. Nanomedicine 9:795–805

43. Chen B, Pogue BW, Zhou X et al (2005) Effect of tumor host microenvironment on photodynamic therapy in a rat prostate tumor model. Clin Cancer Res 11:720–727